


Excitons in InP, GaP, and Ga_xIn_{1-x}P quantum dots: Insights from time-dependent density functional theory

Xiaoyu Ma,¹ Jingjing Min,¹ Zaiping Zeng^{✉,1,*} Christos S. Garoufalidis^{✉,2,†} Sotirios Baskoutas,² Yu Jia,^{1,3,‡} and Zuliang Du¹

¹Key Laboratory for Special Functional Materials of Ministry of Education, Collaborative Innovation Center of Nano Functional Materials and Applications, and School of Materials Science and Engineering, Henan University, Kaifeng, Henan 475001, China

²Materials Science Department, University of Patras, 26504 Patras, Greece

³International Laboratory for Quantum Functional Materials of Henan, and School of Physics and Engineering, Zhengzhou University, Zhengzhou, Henan 450001, China

 (Received 25 August 2019; revised manuscript received 13 November 2019; published 3 December 2019)

Colloidal quantum dots (QDs) of group III-V are considered as promising candidates for next-generation environmentally friendly light emitting devices, yet there appears to be only limited understanding of the underlying electronic and excitonic properties. Using large-scale density functional theory with the hybrid B3LYP functional solving the single-particle states and time-dependent density functional theory accounting for the many-body excitonic effects, we have identified the structural, electronic, and excitonic optical properties of InP, GaP, and GaInP QDs containing up to a thousand atoms or more. The calculated optical gap of InP QD appears in excellent agreement with available experiments, and it scales nearly linearly with the inverse diameter. The radiative exciton decay lifetime is found to increase surprisingly linearly with increasing the dot size. For GaP QDs we predict an unusual electronic state crossover at a diameter of around 1.5 nm, whereby the nature of the lowest unoccupied molecular orbital (LUMO) state switches its symmetry from Γ_5 -like at a larger diameter to Γ_1 -like at a smaller diameter. After the crossover, the absorption intensity of the band-edge exciton states is significantly enhanced. Finally, we find that Vegard's law holds very well for GaInP random alloyed quantum dots down to ultrasmall sizes with less than a hundred atoms. The obtained energy gap bowing parameter of this common-cation compound in QD regime appears positive, size-dependent, and much smaller than its bulk parentage. The volume deformation, dominating over the charge exchange and structure relaxation effects, is mainly responsible for the QD energy gap bowing. The impact of excitonic effects on the optical bowing is found to be marginal. The present work provides a road map for a variety of electronic and optical properties of colloidal QDs in group III-V that can guide spectroscopic studies.

DOI: [10.1103/PhysRevB.100.245404](https://doi.org/10.1103/PhysRevB.100.245404)

I. INTRODUCTION

Colloidal quantum dots (QDs) have demonstrated their great potential in modern light emitting devices [1–3] owing to their high stability, tunable emission spectrum, narrow bandwidth, and broad luminescent spectral range. Light emitting diode (LED) technology based on cadmium selenide (CdSe) QDs of group II-VI has witnessed tremendous development in the last two decades, with both brightness and external quantum efficiency rivaling the state-of-the-art organic light emitting devices [4]. However, the heavy metal-containing feature of these group II-VI QDs is the major obstacle limiting their further development towards commercialization. Colloidal QDs of group III-V compounds (InP, GaP, GaInP, etc.) have been used for a plethora of applications, such as a color converter in a liquid crystal display [5], LEDs [6,7], thin-film transistors [8], and bioimaging [9,10]. Among them, InP is considered as a promising candidate to replace CdSe as a material of choice for commercial QD displays due to its low toxicity [11,12] but comparable, or

even broader emission color range over traditional group II-VI compounds. The other members of the group III-V family such as GaP and GaInP have also seen a significant surge of interest as light emitting materials [13–16]. Even though the synthetic chemistry of colloidal III-V semiconducting QDs has seen significant progress [17–19], the growth of uniform, monodisperse high quality QDs of group III-V remains challenging. This is partly because of the intrinsic more covalent bonding nature of group III-V compounds, and partly due to the lack of appropriate cation and anion precursors with balanced reactivity [20]. The resultant low quality of the fabricated QDs therefore hinders the exploration of their excitonic optical properties, and more broadly limits their device applications.

Modeling of the excitonic properties of a QD requires (i) accurate ground-state electronic structure calculations, which are able to deliver correct band gap and atomistic wave functions, and (ii) accurate treatment of excited state properties. In the former aspect, an atomistic tight-binding method [21–23] and an empirical pseudopotential theory [24–28] are able to describe the electronic properties of QDs from a few hundred atoms to millions of atoms. However, those methods are heavily parametrized, and usually rely on a predefined unrelaxed geometry due to the lack of total

* zaiping.zeng@henu.edu.cn

† garoufal@upatras.gr

‡ jiayu@henu.edu.cn

energy calculations. Continuum models, such as effective-mass approximation and $\mathbf{k} \cdot \mathbf{p}$ theory, are best suited for large QDs, but fail where atomistic effects become important. On the latter aspect, many-body effects play an important role in the excitonic optical properties, such as absorption edge, excitonic polarization, and fine structure. This interaction is largely magnified in a zero-dimensional system due to the combined effects of geometric confinement and reduced screening.

In this work we study theoretically the electronic and excitonic optical properties of colloidal QDs of typical group III-V compounds, such as InP, GaP, and GaInP, employing the ground-state and excited state density functional theory calculations (i.e., DFT and TDDFT). Thanks to the group theory and high-performance computing facilities, we are able to treat realistic QDs with more than 1000 atoms. We have determined a variety of excitonic optical properties of those QDs, including size-dependent optical gap, exciton binding energy, exciton decay lifetime, singlet-triplet splitting, and optical absorption spectrum. In the following section we will outline the computational details. Thereafter, in Sec. III, numerical results and related discussion are presented. Section IV is devoted to conclusions.

II. COMPUTATIONAL DETAILS

The quantum dots (QDs) are cut from the corresponding bulk materials with nearly spherical shape (i.e., characterized by diameter D) and centered at a cation atom. This naturally leads to a T_d point group symmetry for a nearly spherical QD of zinc-blende structure. The sizes of QDs range from 1.07 to nearly 3.5 nm which have a total number of atoms ranging from 65 to 1101 atoms, and therefore are within the strong confinement regime. QDs of such sizes can be synthesized using the well-established modern colloidal fabrication method [29–31]. The surface dangling bonds are passivated with pseudohydrogens, which has modified nuclear charges of 1.25 and 0.75 to terminate surface cations and anions of group III-V (e.g., InP, GaP, etc.), and of 1.5 and 0.5 to terminate their counterparts of group II-VI (e.g., CdSe), respectively. We note that oleate, oleic acids, and hydrofluoric acid are the commonly adopted ligands for the surface passivation of colloidal QDs in the experimental reality. Therefore, the present pseudohydrogen passivation scheme represents a simple model with an ideal ligand, which is known to well reproduce the size-dependent experimental band gaps of various colloidal QDs.

All calculations are performed with the Turbomole suit of programs [32]. The geometry optimization is performed in the framework of density functional theory (DFT) with generalized gradient approximation (GGA) of Perdew-Burke-Ernzerhof (PBE) type [33], which is known to predict rather accurately the structural properties. However, this level of theory is known to underestimate the band gap, and is detrimental for the modeling of optical properties. We therefore employ the hybrid nonlocal exchange-correlation functional of Becke and Lee, Yang, and Parr (B3LYP [34]) to calculate reliably the single-particle HOMO-LUMO gap. We have chosen a basis set of double zeta quality (namely, the def2-SVP basis sets of the Karlsruhe group [35,36]) throughout the work, which

allows for calculations in systems with tens of hundreds of atoms without significantly compromising the accuracy.

The excitonic optical properties are calculated on top of the B3LYP results, using the linear-response time-dependent DFT (TDDFT). We note that the energy of the lowest symmetry-allowed and spin allowed transition (singlet state) is considered as the optical gap regardless of its oscillator strength. The radiative decay lifetime (τ_x) is calculated according to [37,38] $\frac{1}{\tau_x} = \frac{4\alpha E_X n |M_X|^2}{m_0^2 \hbar c^2}$, where n is the refractive index, α is the fine-structure constant, m_0 is the electron rest mass, c is the velocity of light, E_X is the exciton energy, and M_X is the electric dipole moment obtained from the TDDFT calculations. The singlet-triplet splitting is defined as the energy difference between the lowest singlet and triplet states based on the optimized ground-state geometry.

III. RESULTS AND DISCUSSION

A. InP quantum dots

Bulk InP is known to be a direct gap semiconductor with a gap of 1.4236 eV at cryogenic temperature [39]. Bulk VBM is sixfold (without spin-orbit interaction) and of Γ_{5v} symmetry, while the CBM is twofold and of Γ_{1c} symmetry [cf. Fig. 1(a)]. The optimized In-P bond lengths of the interior atoms in the InP QDs at GGA/PBE level of theory are ranging from 2.591 to 2.594 Å, which are nearly identical to that of bulk InP structure (~ 2.598 Å). The charge density distribution of the highest occupied molecular orbital (HOMO) state of InP QDs mainly resides on P atoms, having a p -type character and a Γ_5 -like symmetry similar to its bulk parentage [cf. Fig. 2(a)]. The lowest unoccupied molecular orbital (LUMO) state is contributed from the s orbitals of both In and P atoms [cf. Fig. 2(a)], and the corresponding charge density distribution accumulates around both types of atoms [cf. Fig. 2(a)]. It has a Γ_1 symmetry, having the same symmetry as the bulk CBM [cf. Fig. 1(a)]. The s - p coupling in a bonding/antibonding manner leads to the opening of the electronic band gap of InP QDs. The HOMO state lowers down in energy, and the LUMO state rises up in energy when enhancing quantum confinement effects, as expected. We find that comparing to the HOMO state, its LUMO counterpart varies more significantly in energy, therefore suggesting that the electron is more delocalized and more sensitive to the quantum confinement effects.

We next evaluate the size-dependent band gap of InP QDs. It is known that the size-dependent band gap (E_g) of a QD is simply expressed according to the analytical equation [41,42]

$$E_g = E_{g,\text{bulk}} + C_g/D^\alpha, \quad (1)$$

where $E_{g,\text{bulk}}$ is the bulk band gap, C_g is a proportionality constant, and α is a real number. We study the band gap evolution as a function of the dot size in Fig. 2(b) based on two levels of theory, i.e., single-particle level using DFT with the B3LYP hybrid functional and correlated exciton level employing TDDFT. The exciton effects are neglected at the former level of theory, and they are properly accounted for at the latter level of theory. A side-by-side comparison of the results at both levels of theory allows us to quantify the impact of excitonic effects. We find that the calculated single-particle gaps at DFT level of theory using B3LYP hybrid functional

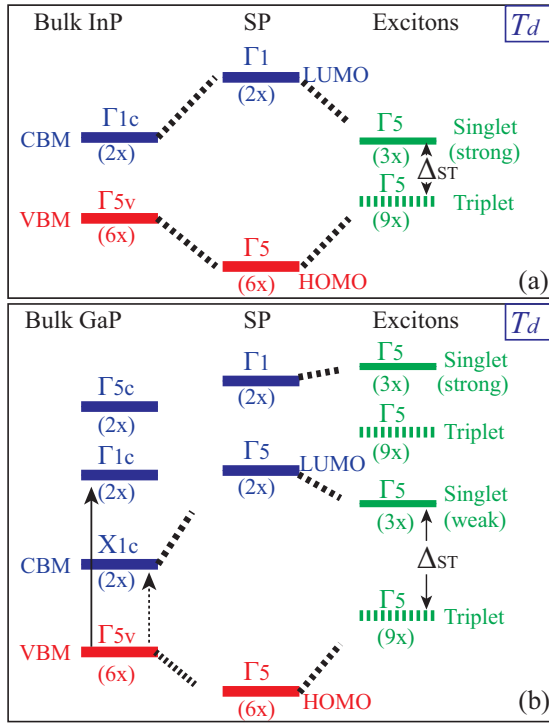


FIG. 1. (a) Symmetry characters of valence band maximum (VBM) and few low lying conduction band states in bulk (a) (left column) InP and (b) (leftmost column) GaP, the HOMO and first few LUMO states of the corresponding quantum dots at the single-particle (SP) level obtained by DFT/B3LYP method (central column), and the resulted exciton manifolds obtained from TDDFT calculations (rightmost column). The degeneracy of the energy levels or exciton states is shown in parentheses. In the leftmost column, the solid vertical arrow indicates an optically allowed transition, while the dashed vertical arrow indicates an optical forbidden one. In the rightmost column, a thick solid horizontal line indicates a symmetry allowed and spin allowed exciton state (singlet state), and a thick dashed horizontal line indicates a symmetry allowed but spin-forbidden exciton state (triplet state). The spin-orbit interaction is neglected but the exchange interaction is considered. We have employed Kosters notations of single group symmetry representations within a T_d point group.

appear slightly larger (~ 0.1 eV) than that reported using HSE06 hybrid functional and plane-wave basis set [31] [cf. Fig. 2(b)]. They are significantly larger than that obtained from eight-band $\mathbf{k} \cdot \mathbf{p}$ theory employing a finite confinement potential [40] [cf. Fig. 2(b)], particularly at small diameters. We note that the gaps calculated using $\mathbf{k} \cdot \mathbf{p}$ theory have been found to be highly dependent on the confinement potential which not only affects the actual gap value but also the size-dependent scaling law of the energy gap (cf. Ref. [40]). This therefore highlights the importance and accuracy of current parameter-free *ab initio* modeling. When considering excitonic effects, we find that the optical gap is systematically lower than the single-particle gap giving a physically consistent picture. This is not always true in DFT calculations, since it is quite common for a pure GGA functional to give TDDFT optical gaps larger than the corresponding single-particle ones. Moreover, the calculated optical gap values compare well with the available experiments [cf.

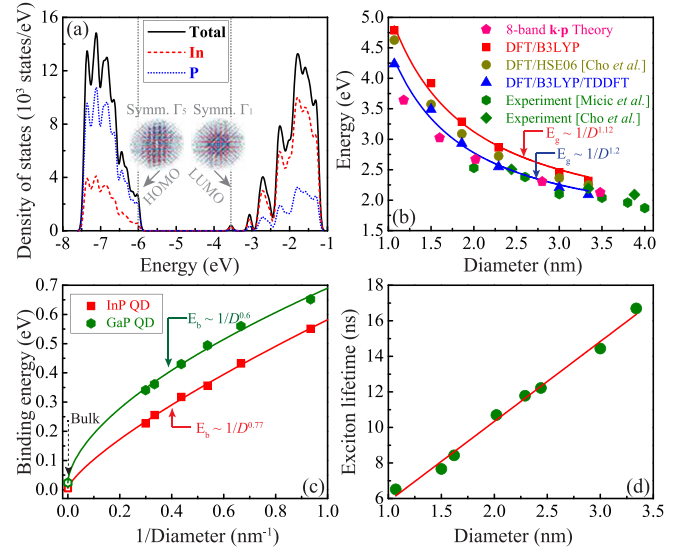


FIG. 2. (a) Atom resolved density of states of InP quantum dots with diameter $D = 3$ nm. The insets show the charge densities of HOMO and LUMO states alongside with their respective point group symmetry. (b) Energy gap as a function of the diameter of InP quantum dots calculated using DFT/B3LYP and DFT/B3LYP/TDDFT, respectively, compared with existing theories and experiments [29,31,40]. Each solid line represents a fit according to Eq. (1). (c) Exciton binding energies as a function of the diameter of InP and GaP quantum dots. (d) Exciton decay lifetime as a function of the diameter of InP quantum dots. The solid line represents a linear fit.

Fig. 2(b)]. The calculated gaps as a function of the dot size is well fitted with the analytical Eq. (1), delivering $C_g = 1.12$ at single-particle level. The excitonic effects turn out to have marginal impact on the scaling law, increasing C_g slightly to 1.2. Those values obtained from the current *ab initio* method differ significantly from that predicted from single-band effective-mass theory using the particle-in-box model ($C_g = 2$), and from that obtained based on large-scale atomistic empirical pseudopotential theory ($C_g = 1.36$) [43]. However, such a nearly linear scaling of energy gaps with respect to the inverse diameter agrees well with the experimental measurements on the core/shell QDs ($C_g \approx 1$) [44].

In contrast to the multiplicity of both experimental and theoretical activities on physical properties in “high energy” (~ 1 eV) scale, the focus on the properties of InP QDs in “low energy” ($\sim 10^{-3}$ eV) scale is rather limited. We therefore study the size dependence of exciton binding energy in InP QDs, which appears in the low energy scale [cf. Fig. 2(c)]. This quantity is defined as the energy difference between the single-particle gap and the optical gap. It has three distinct contributions: (i) electron-hole Coulomb interaction, (ii) electron-hole exchange interaction, and (iii) correlation effects. Among those contributions, the electron-hole Coulomb interaction is the major contribution, and scales as $1/D$. In contrast to the weak binding of excitons in bulk InP ($E_{b,\text{bulk}}^X = 5.1$ meV), excitons under three-dimensional quantum confinement appear to be strongly bound, reaching up to 550 meV for our smallest InP QD. Considering the size-dependent scaling law of the dominant contribution, the calculated exciton binding energy (E_b^X) is expected to be well

fitted using the analytical equation similar to Eq. (1),

$$E_b^X = E_{b,\text{bulk}}^X + C_b^X/D^\beta, \quad (2)$$

with β being a fitting parameter. We find that the exciton binding energy scales as $D^{-0.77}$ [cf. Fig. 2(c)], which again differs from the prediction of effective-mass theory using the particle-in-box model ($E_b^X \propto 1/D$), representing solely the Coulomb interaction between the electron and hole. For comparison purpose, we have also examined the scaling law of size-dependent exciton binding energy for CdSe QDs on an equal footing. It turns out that the calculated exciton binding energy of CdSe QD is very comparable to its InP counterpart of equal size, and it scales as $E_b^X \propto 1/D^{0.72}$, which reproduces exactly the experimentally determined scaling law [45]. We note that the numerically obtained exciton binding energies are significantly smaller than the experiments [45] (not shown), suggesting that the current theoretical scheme may underestimate the exciton binding energy. The optimally tuned time-dependent range-separated hybrid density functional theory [46,47] could offer a better description on the exciton binding energy, but is certainly more computationally demanding.

Finally, we study the size dependence of an exciton decay lifetime of the first-bright exciton state of InP QDs in Fig. 2(d). The obtained lifetime appears at the nanosecond timescale for the sizes considered herein. Strikingly, we find that the lifetime increases monotonically, and scales linearly as a function of the dot size [cf. Fig. 2(d)]. Such a linear behavior has also been experimentally found for CdSe QDs [48]. We find that the lifetime of the first-bright exciton state in InP QD appears systematically larger than that in its CdSe counterpart of equal size and stoichiometry. This is mainly associated with more balanced electron and hole effective masses in bulk CdSe of zinc-blende phase ($m_{e,\text{CdSe}}^* = 0.12m_0$, $m_{hh,\text{CdSe}}^* = 0.33m_0$; $m_{e,\text{InP}}^* = 0.0765m_0$, $m_{hh,\text{InP}}^* = 0.45m_0$, where m_0 is the free electron mass), which causes a larger electron-hole wave function overlapping and therefore a shorter exciton lifetime. We note that the lifetime not only depends on the dot size, but also on the surface inorganic stoichiometry.

B. GaP quantum dots

Gallium phosphide (GaP), as another typical compound of group III-V, is known to be an indirect band gap semiconductor with VBM locating at Γ point and of Γ_5 symmetry, and CBM locating at X point and of X_1 symmetry [cf. Fig. 1(b)]. It has an indirect gap of 2.355 eV [49] and a larger direct gap of 2.895 eV [50] at Γ point measured at cryogenic temperature. GaP therefore has been considered as a promising candidate for a blue fluorophore. However, given its indirect band gap nature, GaP cannot be considered as an efficient photon emitter in bulk at least at cryogenic temperature where phonon-assisted emission is minimal. One way to make GaP relevant as a light-emitting compound is to alleviate the indirect nature of the band structure via quantum confinement effects. Many experimental activities therefore have focused on synthesis of GaP QDs under a strong quantum confinement regime [30,51–55]. Both broad size distribution and the lack of a thorough analysis of the optical properties of the fabricated GaP QDs result in only a rough determination of the corresponding

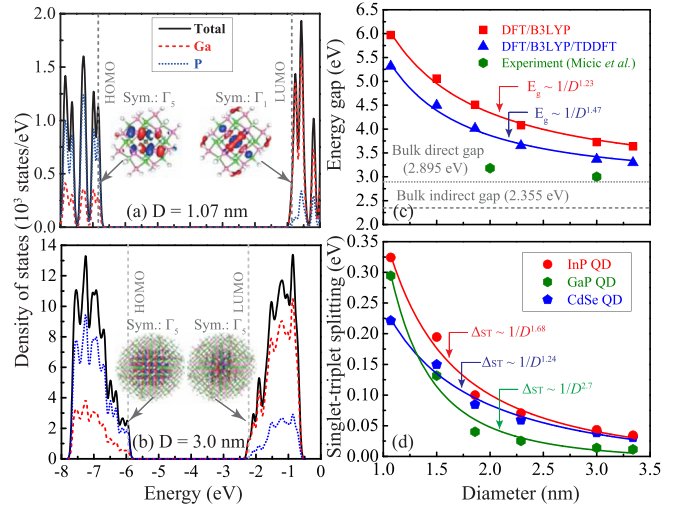


FIG. 3. Atom resolved density of states of GaP quantum dots with diameter (a) $D = 1.07$ nm and (b) 3 nm obtained at DFT/B3LYP level of theory, respectively. The dotted vertical line indicates the energy position of HOMO and LUMO states. The inset shows the charge density of the HOMO and LUMO states alongside the corresponding symmetry character. (c) Energy gap as a function of the diameter of GaP quantum dots calculated using DFT/B3LYP and DFT/B3LYP/TDDFT levels of theory, respectively, compared with existing experiments [30]. Each solid line represents a fit according to Eq. (1). (d) The singlet-triplet splitting Δ_{ST} as a function of the diameter of GaP QDs, compared with that of InP and CdSe QDs. Each solid line represents a fit using equation $\Delta_{ST} = \delta + C_{st}/D^\gamma$, where δ , C_{st} , and γ are fitting parameters.

quantum confinement effects. The reported *ab initio* study has been limited to cluster size [56]. We therefore employ the aforementioned reliable theoretical scheme for the study of InP QDs as a means to gain insights on the excitonic optical properties of GaP QDs of realistic sizes, which have not been treated appropriately either by *ab initio* methods or other suitable approximations such as $\mathbf{k} \cdot \mathbf{p}$ theory.

The optimized Ga-P bond lengths of the interior atoms in the QDs are nearly identical to their bulk parentage (~ 2.3945 Å), regardless of the dot size. The HOMO state of GaP QD always has a dominant contribution from p orbital of P atoms, and inherits the same symmetry character of the corresponding bulk phase [e.g., Γ_5 , cf. Fig. 1(b) and Figs. 3(a) and 3(b)]. In contrast to bulk CBM having a X_1 symmetry, the LUMO state of GaP QD presents a Γ_5 symmetry for larger QDs [e.g., $D = 3$ nm and cf. Fig. 3(b)], which switches to Γ_1 symmetry at ultrasmall sizes [e.g., $D = 1.07$ nm, cf. Fig. 3(a)], therefore recovering the symmetry of bulk CBM at Γ point [cf. Fig. 1(b)]. Such a switching is found to occur at a diameter around 1.5 nm. The switch in the LUMO symmetry can be attributed to the nontrivial interplay between symmetry mixing (or bulk Bloch-band mixing) and quantum confinement effects on the QD conduction-band electronic structure. Such an unconventional behavior has also been found in Si nanowires [38]. The single-particle gap of GaP QD is calculated in Fig. 3(c) as a function of the QD size. It shows that the HOMO-LUMO gap scales as $E_g \propto 1/D^{1.23}$, indicating that GaP QD is more sensitive to the quantum confinement effects than its InP counterpart (e.g., $E_g \propto 1/D^{1.12}$).

The direct transition from HOMO to LUMO states results in a ninefold spin-triplet state (optically dark) at a lower energy, and a threefold spin-singlet state (optically active) at a higher energy [cf. Fig. 1(b)]. All of these exciton states are of Γ_5 symmetry [cf. Fig. 1(b)]. Although being optically allowed, this spin-singlet exciton state exhibits weak transition dipole moment μ_D , and therefore small oscillator strength f_{osc} and long radiative decay time τ_X . This is in stark contrast to that in InP QD. For $D = 1.5$ nm, we find that $\mu_D^{\text{GaP}} = 0.022$ Debye, $f_{\text{osc}}^{\text{GaP}} = 0.00016$, and $\tau_X^{\text{GaP}} = 5.86$ μs . However, for InP QD of equal size, we find that $\mu_D^{\text{InP}} = 1.54$ Debye, $f_{\text{osc}}^{\text{InP}} = 0.56$, and $\tau_X^{\text{InP}} = 7.66$ ns. Concerning the scaling law, we find that the excitonic effects bring the scaling law further apart from linear scaling. The optical gap of GaP QD is found to scale as $E_g^X \propto 1/D^{1.47}$ [cf. Fig. 3(c)]. The calculated optical gap appears significantly larger than the reported experimental data [30] measured at high temperatures [≈ 400 °C, cf. Fig. 3(c)]. The discrepancy shall be partly resolved by future measurements on GaP QDs with narrow size distribution at cryogenic temperatures to exclude both the size uncertainty and the thermal noise.

The exciton binding energy of GaP QD is systematically larger than its InP counterpart. It scales as $E_b^X \propto 1/D^{0.6}$ [cf. Fig. 2(c)], deviating significantly from the linear scaling law governed solely by the Coulomb interaction between the electron and hole. The singlet-triplet splitting Δ_{ST} as a function of the diameter of GaP QDs is studied in Fig. 3(d). The results are compared with that of InP and CdSe QDs. We find that (i) $\Gamma_5 \rightarrow \Gamma_5$ transition resulted exciton manifold appears to have a much smaller Δ_{ST} than that originated from $\Gamma_5 \rightarrow \Gamma_1$ transition. This is evident by comparing the results before ($D > 1.5$ nm) and after ($D < 1.5$ nm) the Γ_5 - Γ_1 electronic state crossover in the LUMO state. (ii) Although both band-edge exciton manifold stemming from Γ_5 - Γ_1 HOMO-LUMO transition, Δ_{ST} in InP QD is systematically larger than that in CdSe counterpart. This is particularly pronounced for smaller diameters. (iii) $\Delta_{\text{ST}} \propto 1/D^{1.68}$ for InP QD and $\propto 1/D^{2.7}$ for GaP QD. This indicates that Δ_{ST} in QDs of group III-V is more size dependent than their group II-VI counterpart (e.g., $\Delta_{\text{ST}} \propto 1/D^{1.24}$ for CdSe QD). We note that the magnitude of Δ_{ST} in a particular QD is determined by the strength of the exchange coupling between the electron and hole states involved in forming the first-bright (or dark) exciton states, which in turn depends on the spatial wave function overlap between them. A larger Δ_{ST} essentially means a smaller overlap between absorption and emission spectrum, which is desirable in applications such as light-emitting diodes, where reabsorption reduces the total efficiency [57].

The absorption spectrum of GaP QDs with various sizes is plotted and compared with that of InP QDs in Fig. 4. Three characteristics are observed: (i) For both types of QDs, the absorption edge blueshifts with enhancing the quantum confinement effects, as expected; (ii) GaP QDs with all sizes exhibit weaker absorption intensity than its InP counterparts, at least at lower energy part of the absorption spectrum; and (iii) the first pronounced exciton absorption peak in both GaP and InP QDs are dominantly contributed from the $\Gamma_5 \rightarrow \Gamma_1$ transition (cf. Fig. 4). For InP QD, such a transition corresponds to the HOMO-LUMO transition, and its intensity increases with *increasing* the dot size due to the

enhancement of overlapping between the HOMO and LUMO wave functions [cf. Figs. 4(a), 4(c), and 4(e)]. For GaP QDs, however, the electron state with Γ_1 symmetry and involved in this transition rises up, going from LUMO+5 at $D = 2.29$ nm to LUMO+2 at $D = 1.07$ nm. In contrast to InP QD, the peak intensity corresponds to such a transition in GaP QDs increases with *decreasing* the dot size [cf. Figs. 4(b), 4(d), and 4(f)]. This remains true for the lower energy part of the absorption spectrum. These results therefore suggest that increasing the quantum confinements can serve as an effective way of enhancing the absorption or PL intensity of GaP QDs. It should be pointed out that the dielectric properties of the solvent could be important as they strongly modify the absorption intensity of the colloidal QD due to the well-known local field effects, but their impact on the optical gap is found to be marginal, at least for the QD sizes considered herein.

C. Ga_xIn_{1-x}P random alloyed quantum dots

After examining the electronic and excitonic optical properties of both InP and GaP QDs, we finally turn to their native ternary alloy Ga_xIn_{1-x}P QDs, which is of technological importance due to the flexibility they offer in terms of band gap and lattice constant engineering. Ga_xIn_{1-x}P QDs emitting green light are expected to be superior to their InP counterparts due to their larger size and correspondingly larger absorption cross sections and smaller surface to volume ratio. Moreover, incorporation of Ga into InP lattice reduces the lattice mismatch with wider band gap shell materials such as ZnS, making the material less strained. This will be beneficial for reducing the trap centers and slowing down Auger recombination rates. Luminescent Ga_xIn_{1-x}P QDs with controlled composition can be well synthesized with the colloidal chemistry method either in molten salts [16] or by suitably choosing a gallium precursor [58].

The lattice constant of bulk ternary compounds (A_xB_{1-x}C) usually varies linearly with composition x , e.g., $a_{\text{alloy}} = xa_{\text{AC}} + (1-x)a_{\text{BC}}$. This is the well-known Vegard's law that is empirical and based purely on observations, but hold surprisingly well for most of the bulk alloyed materials. We therefore first check the validity of Vegard's law when moving from bulk to the nano regime. We have chosen two representative sizes, e.g., $D = 1.62$ and 2.29 nm, with the consideration of computational cost caused by the random geometric configuration averaging. We have employed a GGA/PBE level of theory for the geometry optimization of the alloyed QDs, which often delivers good structural properties. Since the definition of lattice constant is no longer valid in QDs, we therefore tend to calculate the average bond length for all the fully neighbored dot atoms (e.g., excluding the surface dot atoms and the pseudohydrogen atoms), and the results are shown in Fig. 5(c). It is shown that Vegard's law holds well even for those ultrasmall alloyed QDs, irrespectively of dot size. With varying Ga ratio x , we find that the HOMO state keeps its origin [e.g., p orbital of P atoms, cf. Figs. 5(a) and 5(b)], while the LUMO switches from a dominant contribution from s orbital of In atoms at smaller x to a mixed contribution from s orbital of both In and Ga atoms at larger x [cf. Fig. 5(b)]. The energy gap as a function of gallium ratio x at both single-particle level and correlated level is shown in Fig. 5(d). It is found that the energy gaps at both levels

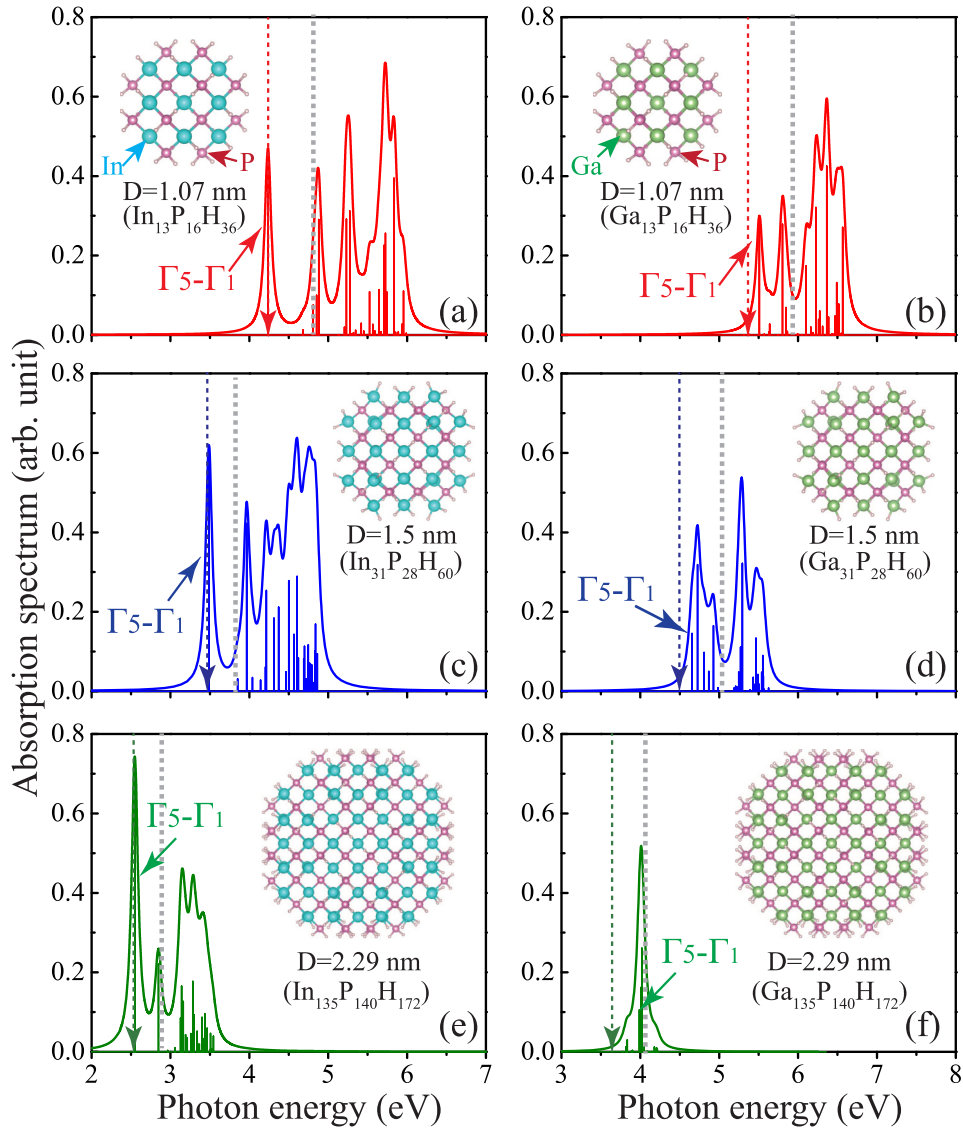


FIG. 4. Absorption spectrum of (a), (c), and (e) InP and (b), (d), and (f) GaP quantum dots with diameter (a) and (b) $D = 1.07$ nm, (c) and (d) 1.5 nm, and (e) and (f) 2.29 nm, respectively, computed on the ground of 30 optically allowed exciton states. The vertical line shows the absorption peak corresponding to each exciton state. A Lorentzian broadening function is employed with broadening parameter $\Gamma_l = 0.05$ eV. The vertical dashed line indicate the single-particle HOMO-LUMO gap, and the vertical arrows show the optical gap. The insets show the geometric structure of the corresponding QD.

experience a monotonic increase with increasing the gallium ratio. A parabola fit of the calculated data enables the determination of the linear coefficient a and the bowing parameter b . We find that the linear coefficients at both single-particle level and correlated level are positive and size dependent. For example, $a = 0.94$ eV at diameter $D = 1.62$ nm and increases to 1.03 eV at $D = 2.29$ nm. Both values experience only a slight decrease to 0.92 and 0.98 eV, respectively, when considering the excitonic effects. Those values in QDs of strong confinement regime appear considerably reduced in comparison to their bulk parentage ($a_{\text{bulk}}^{\Gamma} = 1.25$ eV [59]).

The obtained bowing parameters are also found to be positive and size dependent. For example, at correlated level, $b = 0.16$ eV at $D = 2.29$ nm and reduces to 0.116 eV at $D = 1.62$ nm, both of which are much smaller than the bulk

optical bowing parameter for the direct band gap at Γ -point $b_{\text{bulk}}^{\Gamma} = 0.648$ eV [60]. The energy gap bowing usually can be decomposed into three physically distinct contributions [61]: (i) volume deformation b_{vd} , (ii) charge exchange b_{ce} , and (iii) structure relaxation b_{sr} . To identify the dominant physical contribution for the energy gap bowing of GaInP QD, we evaluate the three contributions according to [61]

$$\begin{aligned}
 b_{\text{vd}} &= \frac{E_{g,\text{RE}}^{\text{GaP}} - E_{g,\text{FX}}^{\text{GaP}}}{1-x} + \frac{E_{g,\text{RE}}^{\text{InP}} - E_{g,\text{FX}}^{\text{InP}}}{x}, \\
 b_{\text{ce}} &= \frac{E_{g,\text{FX}}^{\text{GaP}}}{1-x} + \frac{E_{g,\text{FX}}^{\text{InP}}}{x} - \frac{E_{g,\text{FX}}^{\text{GaInP}}}{x(1-x)}, \\
 b_{\text{sr}} &= \frac{E_{g,\text{FX}}^{\text{GaInP}} - E_{g,\text{RE}}^{\text{GaInP}}}{x(1-x)},
 \end{aligned} \tag{3}$$

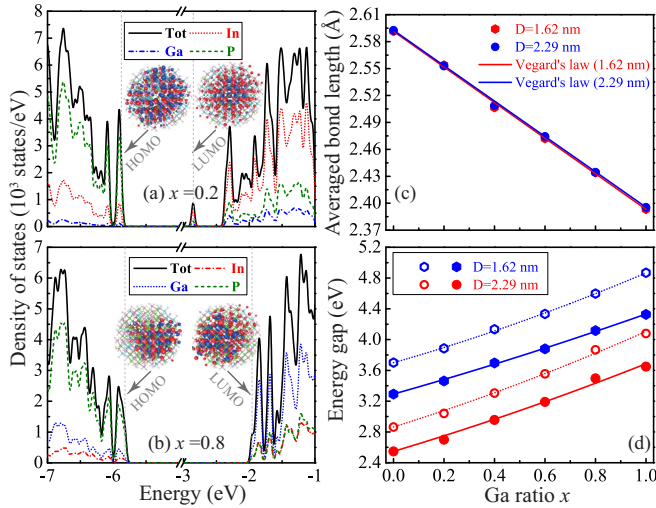


FIG. 5. Density of states of Ga_xIn_{1-x}P alloyed quantum dots of $D = 2.29$ nm with Ga ratio (a) $x = 0.2$ and (b) 0.8 , respectively. The insets show the charge density plots of the HOMO and LUMO states. (c) The averaged bond length (symbols) of GaInP alloyed quantum dot as a function of Ga ratio x for diameter $D = 1.62$ and 2.29 nm, respectively. The solid line represents the expected bond length predicted from Vegard's law using the GGA/PBE calculated average bond lengths of InP and GaP QDs. (d) The single-particle (open symbols) and optical (closed symbols) gaps as a function of Ga ratio x for diameter $D = 1.62$ and 2.29 nm, respectively. The line represents fits according to $E_g = E_g^{\text{InP}} + ax + bx^2$, where a and the bowing parameter b are fitting parameters. In (c) and (d), each data represents the averaged value over ten random geometric configurations.

where E_g^{InP} , E_g^{GaP} , and E_g^{GaInP} are the energy gap of InP, GaP, and Ga_xIn_{1-x}P at fully relaxed (subscript RE) geometry or fixed (subscript FX) geometry. We note that for the fixed geometry, the initial dot structure is cut from the corresponding bulk material with desired lattice constant $a_{\text{Ga}_x\text{In}_{1-x}\text{P}}$ determined by Vegard's law, and then a geometry optimization procedure is applied with the dot atoms being fixed and surface passivating atoms being allowed to be fully relaxed. The energy band gap of the alloyed QD represents the averaged value over ten random geometric configurations. We find that for $D = 1.62$ nm, $b_{\text{vd}} = 0.51$ eV, $b_{\text{ce}} = 0.12$ eV, and $b_{\text{sr}} = -0.33$ eV, respectively, at $x = 0.2$. The sum of these three contribution, $b = b_{\text{vd}} + b_{\text{ce}} + b_{\text{sr}} = 0.3$ eV, well reproduces the numerically obtained bowing parameter [parabolic fit of Fig. 5(d), ~ 0.22 eV]. This therefore suggests that the volume deformation is the dominant contribution responsible for the energy gap bowing of GaInP alloyed QDs. The volume deformation potential at QD regime has been found to be size dependent and significantly reduced comparing to bulk [27,62]. This therefore explains why the bowing parameter of GaInP QD is size dependent and significantly smaller than its bulk parentage.

The absorption spectrum of GaInP QDs with two representative gallium ratio is shown in Fig. 6, which is compared with those of InP and GaP QDs of equal size. Two distinct characteristics are observed: (i) due to the lowering in symmetry, the degenerate excitonic absorption peaks of InP QDs are

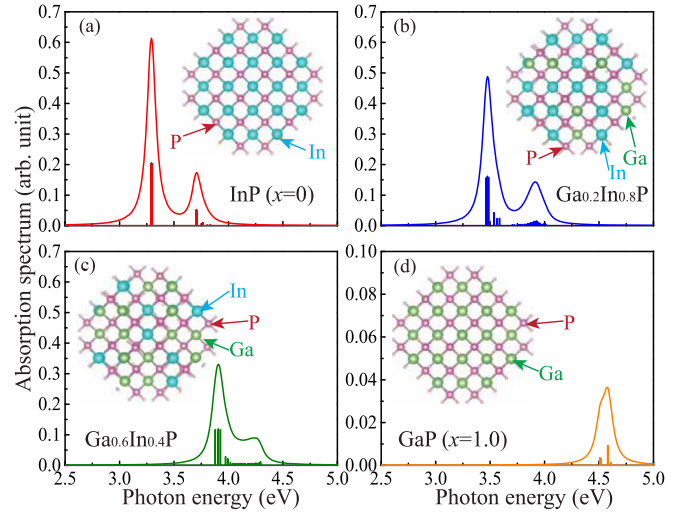


FIG. 6. Absorption spectrum of Ga_xIn_{1-x}P quantum dots of $D = 1.62$ nm with various Ga ratio x calculated with the lowest 40 exciton states without any symmetry constrains (e.g., C_1 symmetry). The vertical line shows the absorption peak corresponding to each exciton state. A Lorentzian broadening function is employed with broadening parameter $\Gamma_l = 0.05$ eV. The inset shows the geometric structure of the QD [in (b) and (c), only one geometric configuration is shown].

split with randomly incorporating Ga atoms into the lattice. The splitting is enhanced when increasing Ga ratio from $x = 0.2$ to 0.6 [cf. Figs. 6(c) and 6(d)]. (ii) The absorption spectrum blueshifts with increasing the Ga ratio. However, the absorption intensity, at least the lower energy part, decreases. Strikingly, we find that the absorption intensity for the first-bright exciton state experiences a sudden drop to nearly zero at $x \approx 0.8$ (not shown), which might be related to switch in the band-edge transition from a $\Gamma_5 \rightarrow \Gamma_1$ transition to a $\Gamma_5 \rightarrow \Gamma_5$ transition. It should be pointed out that the direct gap to indirect gap transition takes place at $x \approx 0.77$ for bulk Ga_xIn_{1-x}P [60].

IV. CONCLUSION

To summarize, we have presented a detailed study of structural, electronic, and excitonic optical properties of InP, GaP, and their ternary compound GaInP QDs of realistic sizes. The electronic structure is calculated using a hybrid functional within density functional theory, while the optical properties are accounted for based on the time-dependent density functional theory. We find that single-particle gap of InP QDs scales nearly linearly as a function of the inverse diameter. The excitonic effects have only a marginal impact on this scaling law, and the calculated optical gaps are found in excellent agreement with available experiments. The exciton binding energy scales as $1/D^{0.77}$, not as $1/D$ as expected, while the radiative exciton decay lifetime is found to increase surprisingly linearly as a function of dot size. For GaP QDs, we have predicted an electron state crossover, whereby the nature of the lowest unoccupied molecular orbital (LUMO) state changes its symmetry from Γ_5 to Γ_1 at a diameter of around 1.5 nm. After the crossover, the pronounced band-edge

exciton state is dominantly contributed from the $\Gamma_5 \rightarrow \Gamma_1$ transition. Both the singlet-triplet splitting and the intensity of the lower energy part of the absorption spectrum experience a significant enhancement with increasing the quantum confinement effects. Finally, we find that Vegard's law holds very well in the GaInP random alloyed quantum dots. The bowing parameter of this common-cation alloyed quantum dot appears size dependent and much smaller than its bulk parentage. The physical mechanism responsible for the energy gap bowing is mainly ascribed to the volume deformation. The excitonic effects are found to have only marginal impact on the energy gap bowing. The current study could be helpful for gaining

insight into the electronic and optical properties of colloidal quantum dots of group III-V towards future optoelectronic applications.

ACKNOWLEDGMENTS

The work has been partly supported by NSFC project with Grants No. 11804077 and No. 11774078, and partly by the innovation research team of science and technology in Henan province (20IRTSTHN020) and the Distinguished Professor grant of Henan University with Grant No. 2018001T.

-
- [1] B. S. Mashford, M. Stevenson, Z. Popovic, C. Hamilton, Z. Zhou, C. Breen, J. Steckel, V. Bulovic, S. Bawendi, S. Coe-Sullivan, and P. T. Kazlas, *Nat. Photon.* **7**, 407 (2013).
- [2] X. Dai, Z. Zhang, Y. Jin, Y. Niu, H. Cao, X. Liang, L. Chen, J. Wang, and X. Peng, *Nature (London)* **515**, 96 (2014).
- [3] S. Chen, W. Cao, T. Liu, S.-W. Tsang, Y. Yang, X. Yan, and L. Qian, *Nat. Commun.* **10**, 765 (2019).
- [4] H. Shen, Q. Gao, Y. Zhang, Y. Lin, Q. Lin, Z. Li, L. Chen, Z. Zeng, X. Li, Y. Jia, S. Wang, Z. Du, L. S. Li, and Z. Zhang, *Nat. Photon.* **13**, 192 (2019).
- [5] J. Owen and L. Brus, *J. Am. Chem. Soc.* **139**, 10939 (2017).
- [6] J. Lim, M. Park, W. K. Bae, D. Lee, S. Lee, C. Lee, and K. Char, *ACS Nano* **7**, 9019 (2013).
- [7] J.-H. Jo, J.-H. Kim, K.-H. Lee, C.-Y. Han, E.-P. Jang, Y. R. Do, and H. Yang, *Opt. Lett.* **41**, 3984 (2016).
- [8] J. Jang, W. Liu, J. S. Son, and D. V. Talapin, *Nano Lett.* **14**, 653 (2014).
- [9] D. J. Bharali, D. W. Lucey, H. Jayakumar, H. E. Pudavar, and P. N. Prasad, *J. Am. Chem. Soc.* **127**, 11364 (2005).
- [10] O. T. Bruns, T. S. Bischof, D. K. Harris, D. Franke, Y. Shi, L. Riedemann, A. Bartelt, F. B. Jaworski, J. A. Carr, C. J. Rowlands, M. W. B. Wilson, O. Chen, H. Wei, G. W. Hwang, D. M. Montana, I. Coropceanu, O. B. Achorn, J. Kloeppe, J. Heeren, P. T. C. So, D. Fukumura, K. F. Jensen, R. K. Jain, and M. G. Bawendi, *Nat. Biomed. Eng.* **1**, 0056 (2017).
- [11] H. Chibli, L. Carlini, S. Park, N. M. Dimitrijevic, and J. L. Nadeau, *Nanoscale* **3**, 2552 (2011).
- [12] G. Lin, Q. Ouyang, R. Hu, Z. Ding, J. Tian, F. Yin, G. Xu, Q. Chen, X. Wang, and K.-T. Yong, *Nanomedicine* **11**, 341 (2015).
- [13] N. Kornienko, D. D. Whitmore, Y. Yu, S. R. Leone, and P. Yang, *ACS Nano* **9**, 3951 (2015).
- [14] J. Sun, C. Liu, and P. Yang, *J. Am. Chem. Soc.* **133**, 19306 (2011).
- [15] B. Lavina, E. Kim, H. Cynn, P. F. Weck, K. Seaborg, E. Siska, Y. Meng, and W. Evans, *Inorg. Chem.* **57**, 2432 (2018).
- [16] V. Srivastava, V. Kamysbayev, L. Hong, E. Dunietz, R. F. Klie, and D. V. Talapin, *J. Am. Chem. Soc.* **140**, 12144 (2018).
- [17] P. Ramasamy, N. Kim, Y.-S. Kang, O. Ramirez, and J.-S. Lee, *Chem. Mater.* **29**, 6893 (2017).
- [18] V. Srivastava, E. Dunietz, V. Kamysbayev, J. S. Anderson, and D. V. Talapin, *Chem. Mater.* **30**, 3623 (2018).
- [19] D. K. Franke, Daniel K. Harris, O. Chen, O. T. Bruns, J. A. Carr, M. W. B. Wilson, and M. G. Bawendi, *Nat. Commun.* **7**, 12749 (2016).
- [20] Z. Xu, Y. Li, J. Li, C. Pu, J. Zhou, L. Lv, and X. Peng, *Chem. Mater.* **31**, 5331 (2019).
- [21] Y. M. Niquet, C. Delerue, G. Allan, and M. Lannoo, *Phys. Rev. B* **62**, 5109 (2000).
- [22] M. Zielinski, *Phys. Rev. B* **86**, 115424 (2012).
- [23] S. Lee, L. Jönsson, J. W. Wilkins, G. W. Bryant, and G. Klimeck, *Phys. Rev. B* **63**, 195318 (2001).
- [24] L.-W. Wang and A. Zunger, *Phys. Rev. B* **53**, 9579 (1996).
- [25] A. Franceschetti, H. Fu, L. W. Wang, and A. Zunger, *Phys. Rev. B* **60**, 1819 (1999).
- [26] S. Baskoutas and G. Bester, *J. Phys. Chem. C* **114**, 9301 (2010).
- [27] Z. Zeng, C. S. Garoufalis, S. Baskoutas, and G. Bester, *Phys. Rev. B* **87**, 125302 (2013).
- [28] Z. Zeng, C. S. Garoufalis, S. Baskoutas, Y. Jia, and G. Bester, *Phys. Rev. B* **98**, 235410 (2018).
- [29] O. I. Micic, H. M. Cheong, H. Fu, A. Zunger, J. R. Sprague, A. Mascarenhas, and A. J. Nozik, *J. Phys. Chem. B* **101**, 4904 (1997).
- [30] O. Micic and A. Nozik, *J. Lumin.* **70**, 95 (1996).
- [31] E. Cho, H. Jang, J. Lee, and E. Jang, *Nanotechnology* **24**, 215201 (2013).
- [32] TURBOMOLE V7.3 2018, a development of University of Karlsruhe and Forschungszentrum Karlsruhe GmbH, 1989–2007, TURBOMOLE GmbH, since 2007; available from <http://www.turbomole.com>.
- [33] J. P. Perdew, K. Burke, and M. Ernzerhof, *Phys. Rev. Lett.* **77**, 3865 (1996).
- [34] P. J. Stephens, F. J. Devlin, C. F. Chabalowski, and M. J. Frisch, *J. Phys. Chem.* **98**, 11623 (1994).
- [35] F. Weigend and R. Ahlrichs, *Phys. Chem. Chem. Phys.* **7**, 3297 (2005).
- [36] F. Weigend, *Phys. Chem. Chem. Phys.* **8**, 1057 (2006).
- [37] D. L. Dexter, *Solid State Physics* (Academic, New York, 1958).
- [38] L. Zhang, J.-W. Luo, A. Franceschetti, and A. Zunger, *Phys. Rev. B* **84**, 075404 (2011).
- [39] H. Mathieu, Y. Chen, J. Camassel, J. Allegre, and D. S. Robertson, *Phys. Rev. B* **32**, 4042 (1985).
- [40] H. Fu, L.-W. Wang, and A. Zunger, *Phys. Rev. B* **57**, 9971 (1998).
- [41] L. E. Brus, *J. Chem. Phys.* **80**, 4403 (1984).

- [42] K. K. Nanda, F. E. Krus, and H. Fissan, *Nano Lett.* **1**, 605 (2001).
- [43] H. Fu and A. Zunger, *Phys. Rev. B* **56**, 1496 (1997).
- [44] A. Narayanaswamy, L. F. Feiner, A. Meijerink, and P. J. van der Zaag, *ACS Nano* **3**, 2539 (2009).
- [45] R. W. Meulenbergh, J. R. Lee, A. Wolcott, J. Z. Zhang, L. J. Terminello, and T. van Buuren, *ACS Nano* **3**, 325 (2009).
- [46] S. Refaely-Abramson, S. Sharifzadeh, N. Govind, J. Autschbach, J. B. Neaton, R. Baer, and L. Kronik, *Phys. Rev. Lett.* **109**, 226405 (2012).
- [47] S. Refaely-Abramson, M. Jain, S. Sharifzadeh, J. B. Neaton, and L. Kronik, *Phys. Rev. B* **92**, 081204(R) (2015).
- [48] Y. Gao and X. Peng, *J. Am. Chem. Soc.* **137**, 4230 (2015).
- [49] R. G. Humphreys, U. Rössler, and M. Cardona, *Phys. Rev. B* **18**, 5590 (1978).
- [50] D. F. Nelson, L. F. Johnson, and M. Gershenson, *Phys. Rev.* **135**, A1399 (1964).
- [51] Y.-H. Kim, Y.-w. Jun, B.-H. Jun, S.-M. Lee, and J. Cheon, *J. Am. Chem. Soc.* **124**, 13656 (2002).
- [52] S. Kher and R. Wells, *Chem. Mater.* **6**, 2056 (1994).
- [53] S. Gao, J. Lu, N. Chen, Y. Zhao, and Y. Xie, *Chem. Commun.*, 3064 (2002).
- [54] F. S. Manciu, Y. Sahoo, D. J. MacRae, M. Furis, B. D. McCombe, and P. N. Prasad, *Appl. Phys. Lett.* **82**, 4059 (2003).
- [55] S. Kim, K. Lee, S. Kim, O.-P. Kwon, J. H. Heo, S. H. Im, S. Jeong, D. C. Lee, and S.-W. Kim, *RSC Adv.* **5**, 2466 (2015).
- [56] C. Kamal, T. K. Ghanty, A. Banerjee, and A. Chakrabarti, *J. Chem. Phys.* **130**, 024308 (2009).
- [57] J. Hu, L.-s. Li, W. Yang, L. Manna, L.-w. Wang, and A. P. Alivisatos, *Science* **292**, 2060 (2001).
- [58] K. D. Wegner, S. Pouget, W. L. Ling, M. Carriere, and P. Reiss, *Chem. Commun.* **55**, 1663 (2019).
- [59] H. Lee, M. V. Klein, L. P. Fu, G. D. Gilliland, H. P. Hjalmarson, D. E. Aspnes, K. C. Hsieh, J. Kim, J. G. Yu, and M. G. Craford, *Phys. Rev. B* **51**, 4186 (1995).
- [60] P. Merle, D. Auvergne, H. Mathieu, and J. Chevallier, *Phys. Rev. B* **15**, 2032 (1977).
- [61] J. E. Bernard and A. Zunger, *Phys. Rev. B* **34**, 5992 (1986).
- [62] Z. Zeng, C. S. Garoufalis, S. Baskoutas, and G. Bester, *J. Chem. Phys.* **142**, 114305 (2015).